

Testing broad line region models with Reverberation mapping

Hagai Netzer^{1*}

¹*School of Physics and Astronomy, Tel-Aviv University, Tel-Aviv 69978, Israel*

9 April 2024

ABSTRACT

New reverberation mapping (RM) measurements, combined with accurate luminosities and line ratios, provide strong constraints on the location of the line emitting gas in the broad line region (BLR) of active galactic nuclei (AGN). In this paper I present new calculations of radiation pressure and magnetic pressure confined clouds and apply them to a “generic AGN” and to NGC 5548. The new calculations are in good agreement with the observed lags of all broad emission lines, and with the luminosities of $\text{Ly}\alpha$, $\text{C IV } 1549$, $\text{O VI } 1035$ and $\text{He II } 1640$. They are also in reasonable agreement with the luminosities of $\text{Mg II } 2798$ and the 1990\AA blend of C III] and Si III] lines for high metallicity gas. They explain the changes in time-lag following an increase in continuum luminosity and their dependencies on the inner and outer boundaries of the BLR. They also predict very strong Balmer and Paschen continua with important implications to continuum RM experiments. However, the calculated Balmer and Paschen line luminosities are too weak, by factors of 2-5. This “Balmer line crisis” was noted in several earlier works and is now confirmed and constrained by RM measurements that were not available in the past. It seems that present photoionization codes that use the escape probability formalism, fail to correctly compute the Balmer line luminosities in high density, large optical depth gas.

Key words:

(galaxies:) quasars: general; (galaxies:) quasars: supermassive black holes; galaxies: nuclei; galaxies: actives

1 INTRODUCTION

High density gas on a sub-pc scale, next to active black holes (BHs) in the centers of active galactic nuclei (AGN), has been studied for years (see e.g. detailed review and numerous references in Netzer 2013). The time variable emission lines from the broad line region (BLR), together with the variable optical-UV-X-ray continuum, are the most recognized signatures of activity in type-I AGN, those sources with a clear view of the vicinity of the BH. Observations of strong, broad, semi-forbidden lines, such as $\text{C III] } 1909$, suggest that the lowest density of the gas is about $n_{\text{H}}=10^{9-10} \text{ cm}^{-3}$, where n_{H} is the hydrogen particle density. The upper limit on the density is not well determined and densities as high as 10^{13} cm^{-3} have been proposed. .

Progress in reverberation mapping (RM) of the BLR gas provides an opportunity to map the location and motion of the gas, and to estimate the BH mass (M_{BH}). RM measurements are now available for a large number of broad emission lines: $\text{H}\alpha$, $\text{H}\beta$, $\text{Ly}\alpha$, $\text{C IV } 1549$, $\text{He II } 1640$, $\text{He II } 4686$, $\text{Mg II } 2798$, and several blends of Fe II lines (Kaspi et al. 2000; Bentz et al. 2010, 2013; Hu et al. 2015; Du et al. 2015; Grier et al. 2017; Pei et al. 2017; Lira et al. 2018; Kriss et al. 2019). They have been used to derive the “mean emissivity radius” (R_{ME}) and the “mean responsivity radius” of many lines, and to demonstrate that these radii increase roughly in proportion to $L_{5100}^{1/2}$, where L_{5100} is the monochromatic continuum luminosity at 5100\AA in erg s^{-1} . For sources in the range $10^{44} < L_{\text{AGN}} < 10^{46} \text{ erg s}^{-1}$, where L_{AGN} is the bolometric luminosity of the source, the mean emissivity radius of the $\text{H}\beta$ line (hereafter $R_{\text{H}\beta}$) is about $34[L_{5100,44}]^{1/2}$ light days (ld), where

* E-mail: hagainetzer@gmail.com

$L_{5100,44} = L_{5100} / 10^{44} \text{ erg s}^{-1}$ (Kaspi et al. 2000; Bentz et al. 2013). RM studies also show different R_{ME} for different lines, starting from the He II lines (about 20-50% of $R_{H\beta}$), going through Ly α and C IV 1549 (about 50-80% of $R_{H\beta}$), other Balmer lines (similar but not always identical to $R_{H\beta}$), and to the Fe II and Mg II lines (somewhat larger than $R_{H\beta}$ with a large uncertainty).

Dust RM experiments, comparing V and K-band luminosity variations, as well as K-band interferometry, provide additional information about the location of the outer boundary of the BLR, R_{out} , identified with graphite grains sublimation radius and the inner walls of a central dusty torus. Earlier theoretical ideas suggested a well defined sublimation radius associated with the inner walls of the central dusty torus, (e.g. Netzer 2015, and references therein). However, it is now clear that grain size and composition play important roles in setting R_{out} (see the detailed study by Baskin & Laor 2018). Moreover, the exact torus geometry plays an important role too and makes it difficult to convert the delayed K-band emission to R_{out} (e.g. Stalevski et al. 2012; Goad & Korista 2015). However, the good agreement between the dust location derived from RM measurements (Koshida et al. 2014), and the location inferred from the K-band interferometry by GRAVITY (Dexter et al. 2020), indicate that geometry and complicated light-echo effects may not be very important. The observations obtained so far suggest $R_{\text{out}}/R_{H\beta} \approx 4$. This $R_{\text{out}}/R_{H\beta}$ is somewhat larger than the one calculated by Baskin & Laor (2018) for the case of isotropic emission ($R_{\text{out}}/R_{H\beta} = 1.5 - 3$). Since R_{out} depends on L_{AGN} and $R_{H\beta}$ depends on L_{5100} , there is an additional ambiguity due to uncertainties on the spectral energy distribution (SED) of such sources, especially the spectral shape of the ionizing continuum.

In this paper I present new, global BLR photoionization models and confront them with measured luminosities and mean emissivity radii of several broad emission lines. Most calculations pertain to an “RM-sample AGN”: an object representing those sources with reliable, multi-season RM measurements. Of the few available global BLR models, none takes into account, in detail, the role of radiation pressure force and none attempts to explain both the gas distribution, as derived from RM measurements, and the luminosities of the strongest lines. As argued below, radiation pressure confined (RPC) cloud models provide the best agreement between line luminosity and line lag except for the Balmer lines. This may indicate a fundamental difficulty in the calculations of these lines. In §2 I describe current BLR cloud models. In §3 I present new photoionization calculations and in §4 I compare them with AGN observations. §5 presents a discussion of the new findings with emphasis on the “Balmer lines crisis”. Throughout this work I assume a standard cosmological model with $\Omega_{\Lambda} = 0.7$, $\Omega_m = 0.3$, and $H_0 = 70 \text{ km s}^{-1} \text{ Mpc}^{-1}$.

2 GLOBAL BLR MODELS

Three generic cloud models have been proposed, over the years, to describe the space and density distribution of the gas in the BLR: magnetic pressure confined (MPC) clouds, locally optimally emitting clouds (LOC), and RPC clouds. Most of this work concerns with the case of *pure* cloud models, where only one type of clouds occupy the entire volume. Several continuous flow wind-type models have also been proposed but without specific calculations of the emitted spectrum. Such models will not be discussed here.

Given L_{AGN} , continuum SED, and gas metallicity, the complete definition of a cloud model requires 6-8 parameters. Five of these are common to all models: the inner and outer radii, R_{in} and R_{out} , the column density of the clouds, N_{col} , and two parameters that define the radial dependence of the global covering factor, C_f ,

$$dC_f = c_1 R^{-p} dR, \quad (1)$$

where c_1 is the covering factor normalization. The line luminosity is obtained by computing the line efficiency coefficient per unit covering factor, $\epsilon(\text{line}, R)$, such that $dL(\text{line}, R) \propto \epsilon(\text{line}, R) dC_f$.

In reality, R_{out} is the dust sublimation radius which is determined by the source luminosity, grain size, and metallicity (see Netzer & Laor 1993; Netzer 2015; Baskin & Laor 2018), and is thus not a free parameter. In this work I assume $R_{\text{out}} = 4R_{H\beta}$ (see discussion below). I also fix the inner BLR boundary to $R_{\text{in}} = 0.2R_{H\beta}$ which is consistent with the shortest observed emission-line time-lag. The exact value affects mostly the luminosity of lines from highly ionized species, like O VI 1035, and the change in R_{ME} in response to continuum variations (§4 below). As detailed below, between two and three additional parameters are required to characterize the gas density, n_{H} , and/or gas pressure, P_{gas} .

The purpose of this work is to calculate the mean emissivity radius (R_{ME}), and luminosity, of various emission lines and compare them with the results of RM experiments and BLR spectroscopy. This is easily done if $\epsilon(R)$ is a powerlaw in radius, $\epsilon \propto R^q$. Here $q = 0$ represents the case where the emitted flux in the line is proportional to the incident continuum flux in exactly the same way at all distances¹. Given this definition, and defining $t = p - q$,

$$R_{\text{ME}} = \frac{\int_{R_{\text{in}}}^{R_{\text{out}}} R^{1-t} dr}{\int_{R_{\text{in}}}^{R_{\text{out}}} R^{-t} dr} = R_{\text{in}} \frac{1-t}{2-t} \frac{[(R_{\text{out}}/R_{\text{in}})^{2-t} - 1]}{[(R_{\text{out}}/R_{\text{in}})^{1-t} - 1]}, \quad (2)$$

for $t \neq 1$ and $t \neq 2$. As shown in several earlier works (e.g. Goad & Korista 2015), and in the following sections of this paper, such a power-law dependence of the line efficiency on R is highly simplified and there is no replacement for real, step-by-step calculations of the emitted spectrum. The

¹ $\epsilon(R)$ can be viewed as a linear responsivity factor analog to the powerlaw responsivity $\eta(R)$ used in other papers ($L_{\text{line}} \propto L_{\text{cont}}^{(R)} \eta(R)$). $q = 0$ corresponds to $\eta = 1$

mean emissivity radius of the *total* line and continuum emission is, however, easier to calculate since in this case $q = 0$ and $t = p$. As shown below, information from the measured luminosities and lags of $\text{Ly}\alpha$, C IV 1549, the Balmer lines and the Balmer continuum, all suggest that in many AGN $p \geq 2$. Note also that R_{ME} depends both on R_{in} and R_{out} , an important issue which is discussed below.

MPC clouds have been suggested by Rees, Netzer & Ferland (1989) and further discussed in Netzer (1990); Goad, O'Brien & Gondhalekar (1993); Kaspi & Netzer (1999); Bottorff et al. (2002); Netzer (2015); Lawther et al. (2018). Such clouds are confined by the pressure of the external magnetic field, P_{mag} , assumed to originate from the central accretion disk (AD). If $P_{\text{mag}} \gg P_{\text{rad}}$, we get $P_{\text{gas}} = P_{\text{mag}}$. The properties of magnetically confined clouds are very similar to the hot-gas confined clouds discussed in Stern et al. (2016). All published BLR models investigated so far assumed a simple radial dependence of the pressure, $P_{\text{mag}} = c_2 R^{-s}$, where c_2 is the (unknown) pressure normalization and s is in the range 0-2. Thus, the total number of parameters in the MPC cloud model, not counting R_{out} , is 6.

MPC clouds are confined on all sides and there is no specific limit on their column density. Some MPC models are normalized in such a way that the column density is large enough to make the back of the cloud almost completely neutral (e.g. Netzer 1990; Kaspi & Netzer 1999). Others (Goad et al. 1993; Lawther et al. 2018) allow matter bounded clouds that are optically thin to the Lyman continuum radiation. The additional assumption that the clouds retain their mass as they move in or out, provides a way to define N_{col} as a function of radius. For gravitationally bounded MPC clouds, $v_{\text{cloud}} \propto R^{-1/2}$ and $p = 2/3s - 3/2$ (Rees et al. 1989) reducing the number of free parameters to 5. Detailed applications of the MPC cloud model to the specific case of NGC 5548, are discussed in Kaspi & Netzer (1999), and Lawther et al. (2018).

LOC models have been proposed by Baldwin et al. (1995) and studied in numerous publications (e.g. Korista et al. 1997; Korista & Goad 2000; Bottorff et al. 2002; Goad & Korista 2015; Korista & Goad 2019). The model assumes a range of densities at any given location and is based on the idea that the escaping radiation from a given location is dominated by line and continuum emission from clouds whose density is close to the density of the highest line production efficiency. The column density of the clouds in most of the published models is constant, in the range $10^{23} - 10^{24} \text{ cm}^{-2}$, and the clouds are not confined. The local density in the LOC model is assumed to be distributed over a large range, $\sim 10^7 - 10^{14} \text{ cm}^{-3}$, and is defined by a power-law distribution with three parameters: $n_{\text{H}}(\text{min})$, $n_{\text{H}}(\text{max})$ and the power-law index which in most LOC models is set to -1. Given this prescription, the number of parameters in LOC models, not counting R_{out} , is 7.

RPC models have been proposed by Dopita et al. (2002) and have been applied first to the dusty, narrow line region (NLR) gas. In this case, the luminosity of the central

source, assumed to be the only source of external pressure, provides radiation pressure force that compresses the dusty gas to a density where $P_{\text{rad}} = P_{\text{gas}}$ at $\tau(\text{Lyman}) \sim 1$. The resulting density is proportional to R^{-2} which gives a constant ionization parameter: $U = Q(\text{Lyman}) / (4\pi R^2 c)$, where $Q(\text{Lyman})$ is the total number of ionizing photons per second and c is the speed of light. For the dusty NLR gas, $\log U \sim -1.5$. Radiation pressure compression is not important in those locations where $P_{\text{gas}}(R) > P_{\text{rad}}(R)$.

Baskin, Laor & Stern (2014) (hereafter BLS14) applied the radiation pressure confinement idea to large column density, dust-free BLR clouds. They showed that in all locations where $P_{\text{rad}} \gg P_{\text{gas}}$ at the illuminated face of the cloud, $L/\text{Ledd} < 1$, and the column density is large enough to keep the material at the back of the cloud neutral, the gas motion is dominated by gravity and the clouds maintain a simple hydrostatic structure. Since $P_{\text{rad}} \propto R^{-2}$, this is the case for *all clouds*, regardless of their distance from the central source, provided the ambient density is low enough. In this model, the ionization parameter inside the clouds, near the hydrogen ionization front, is $\log U \sim -1$. Further study of this model is given in Stern et al. (2016).

The structure of RPC clouds change significantly when the column density drops below a certain value which, for the SED considered by BLS14, is *few* $\times 10^{23}$. The radial structure and the motion of such clouds is determined by the combined effects of radiation pressure and gravity. Examples of such motion are given in Netzer & Marziani (2010). For a large enough N_{col} , the number of parameters in the RPC model not counting R_{out} is 5.

BLS14 did not address the case where high density gas in some parts of the BLR result in $P_{\text{gas}} > P_{\text{rad}}$. They also did not consider the case where the local properties of the clouds are determined by some combination of P_{rad} and P_{mag} , or the case where there is not enough gas, in some directions, to result in optically thick RPC clouds. They made no attempt to match RPC cloud models to RM measurements but line luminosities were roughly compared with typical equivalent widths in order to estimate C_f .

The main premise of the RPC model contradicts some of the assumptions of both the LOC and MPC models. In the LOC case, gas whose density is such that $P_{\text{rad}} > P_{\text{gas}}$, and its column density large enough, will be compressed on a short time scale and its contribution to the local line emission will differ, substantially, from what is assumed by the model. This is also the case in the MPC clouds model in those locations where $P_{\text{rad}}(R) \geq P_{\text{mag}}(R)$.

The recent progress in RM experiments (§1) resulted in a large number of AGN with known BH mass, luminosity and lag for several emission lines, and graphite sublimation radius. Such observations can be used to put strong observational constraints on the distribution of the BLR gas and to test the various global cloud models. Several attempts of this type, focusing on the well studied case of NGC 5548 and using the MPC and LOC cloud models, have been published (Kaspi & Netzer 1999; Lawther et al. 2018; Bottorff et al. 2002; Korista & Goad 2019). However, none included the

inevitable influence of the radiation pressure force. Below I use new photoionization calculations to explore various RPC and MPC cloud models. I do not include LOC models which are inconsistent with the basic assumption of the RPC model.

3 MULTI-CLOUD PHOTOIONIZATION MODELS

3.1 Spectral energy distribution and gas composition

The present calculations apply to a generic RM-sample AGN whose broad emission line spectrum is the mean of the population in terms of line luminosity and line time-lag. This includes sources with $L_{5100,44}=0.1-10$. The central source of radiation is assumed to be an optically thick accretion flow, either a geometrically thin AD like the ones calculated by Slone & Netzer (2012) but without a disk wind, or a yet unexplained flow with a different SED. The mass of the central BH is assumed to be $M_{\text{BH}}=10^8 M_{\odot}$ but this plays a minor role in the present work.

Four different SEDs are considered. Two represent standard geometrically thin ADs with different accretion rates and spin parameter (a): one with $a = 0.7$ and radiation conversion efficiency $\eta = 0.104$ (hereafter AD1) and one with $a = -1$ and $\eta = 0.038$ (hereafter AD2). The accretion rates are determined by the requirement that $L_{5100}=10^{44} \text{ erg s}^{-1}$. This results in $R_{H\beta}=34L_{5100,44}^{1/2} \text{ ld}$. The corresponding Eddington ratios (L/L_{Edd}) are 0.108 and 0.045.

The two disk SEDs are combined with a 0.5-100 keV X-ray powerlaw continuum with an energy index of $\alpha_X=0.9$. The optical-to-X-ray index (α_{OX}) is 1.38 for AD1 and 1.55 for AD2. None of the results pertaining to the RM-sample AGN are sensitive to the exact X-ray properties. Given these SEDs, the mean energies of the ionizing photons are 2.16 Rydberg for AD1 and 1.8 Rydberg for AD2. The ionizing luminosities are $10^{45} \text{ erg s}^{-1}$ and $10^{44.34} \text{ erg s}^{-1}$, respectively.

For proper comparison with earlier BLR models and SEDs, I also considered two broken powerlaw SEDs with properties similar to those considered in the literature. The first is characterized by a $L_{\nu} \propto \nu^{-1.6}$ Lyman continuum and an IR-optical-UV continuum which is a combination of powerlaws with slopes 0.5 and 1. The X-ray continuum is similar to the one assumed for the accretion disks. The fourth SED is the one observed for NGC 5548 during 2014 (Mehdipour et al. 2015) with $L_{\text{ion}}=10^{44.34} \text{ erg s}^{-1}$, $Q(\text{H})=1.29 \times 10^{54}$, $L_{\text{AGN}}=10^{44.44} \text{ erg s}^{-1}$, and $L_{5100}=10^{43.37} \text{ erg s}^{-1}$.

Table 1 provides information about the different SEDs and Fig. 1 shows all four of them. The table lists L_{ion}/L_{5100} , mean energies of ionizing photons in Rydberg, and α_{OX} . The first of those is very important since most of the properties discussed in this work are determined by L_{ion} yet the common normalization in RM studies is relative to L_{5100} .

Line luminosities depend also on the gas composition. In the present work this is taken to be one of the default

Table 1. SED properties

SED	$L_{\text{ion}}/L_{\text{op}}$	Mean E(Ryd)	α_{OX}
AD1	10	2.16	1.38
AD2	2.2	1.80	1.55
Powerlaw	3.4	3.20	1.39
NGC 5548	9.2	7.8	1.27

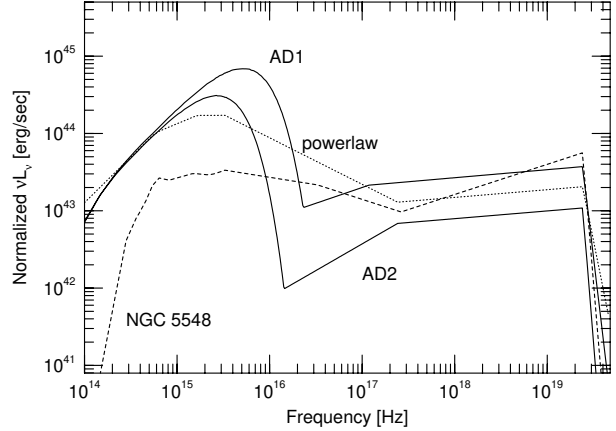


Figure 1. Various SEDs used in this work.

AGN compositions provided by *cloudy*:

(H : He : C : N : O : Ne : Mg : Al : Si : S : Ar : Ca : Fe) =
 $10^{-4} \times (10^4 : 10^3 : 2.45 : 0.85 : 4.9 : 1.0 : 0.347 : 0.0234 : 0.347 : 0.177 : 0.025 : 0.023 : 0.282)$

One of the cases presented below assumes metallicity which is three times higher. For all elements, excluding nitrogen and helium, this is obtained by simply multiplying the abundance by 3. For nitrogen which is a secondary element, I multiply the above number by 6.4.

3.2 Photoionization codes

Most of the models presented below were calculated using version C17.01 of the code *cloudy* (Ferland et al. 2017). BLS14 used version 10 of the code. They assumed a low starting density, well below the density where $P_{\text{rad}}=P_{\text{gas}}$, and integrated until the material becomes completely neutral. This is reached at a column density of $\text{few} \times 10^{23} \text{ cm}^{-2}$. In the present calculations I used $N_{\text{col}}=10^{23.5}$. The exact value of N_{col} makes little difference to the line intensities provided the back of the cloud is more than 95% neutral. While the column density is very large, the ionized parts of the clouds are significantly smaller, with $N_{\text{col}}=10^{23} \text{ cm}^{-2}$ or less. Thus, the Compton depth, and the optical depth at the various hydrogen bound-free edges, do not depend much on the exact choice of N_{col} .

A problem which was encountered by BLS14, is the dis-

ruption of the clouds by the internal line radiation pressure. This instability, which is also encountered in *cloudy* C17.01, is not very important since RPC clouds are not confined in the lateral direction and hence will likely change their shape, on a sound speed crossing time, to compensate for this effect. However, the instability can cause the calculations to crash. Because of this, BLS14 shut-off the internal line radiation pressure (by using the command *no radiation pressure*). Experimenting with RPC models that do not result in such crash shows that the internal density and temperature structures of the clouds are considerably different, but the emergent line flux is hardly affected. All this is discussed and demonstrated in BLS14. Most cases shown below are taken from *cloudy* calculation without including line radiation pressure.

Since *cloudy* is basically the only code used in recent years to calculate BLR models, I used the code ION, most recently described in Mor & Netzer (2012), to complement and verify the results. The current version, ION2019, contains all the physical processes included in *cloudy* except for the treatment of molecular gas. The atomic data set is less complete but is fully updated for the lines considered here and for the main coolants of the gas. The hydrogen atom scheme used in ION2019 contains fewer levels but the number is large enough, and the conditions far enough from LTE, such that the emergent hydrogen spectrum is very similar to the one calculated by *cloudy*. A more fundamental issue is the treatment of HeI and HeI-like ions where the *cloudy* scheme contains many more levels and a full *n-l* treatment. This is not included in ION2019 and hence the resulting HeI spectrum is less reliable. These lines are not included in the present work and are also not very important in controlling the gas temperature. ION includes also the treatment of line radiation pressure but the process does not cause any instability, probably because the number of lines, and the exact treatment of photon escape, are different from those used in *cloudy*. Here, again, I verified that shutting off this process makes only a small difference to the emergent line flux.

Fig. 2 shows a comparison of the H β , Ly α , C IV 1549 and He II 1640 calculations made by the two codes for the basic RPC-AD1 model described below, over a large range of distances. The differences in all cases are below 0.15 dex and there is no systematic trend. A comparison of several MPC cloud models, not shown here, show them to be in very good agreement too. The only significant difference (~ 0.2 dex) is found for the C IV 1549 line in the AD2 model. I have also compared the density and temperature run inside the cloud and found very small differences. The small difference in the Lyman and Balmer lines between the two codes are probably due to the somewhat different expressions used to calculate the local escape probability for the lines. These are well known issues which are not directly related to the more fundamental uncertainties associated with the hydrogen line transfer discussed in §5 below. For the rest of this paper, all results shown are those calculated using *cloudy*.

BLS14 did not address the comparison of the integrated line emission, and mean emissivity radii, with observations. They only show line intensities at various distances from the

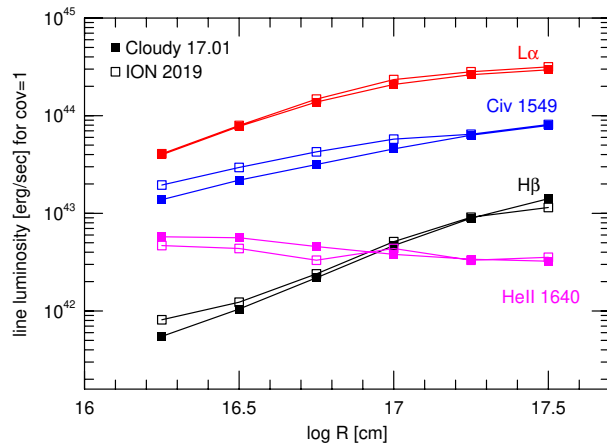


Figure 2. Comparison of *cloudy* C17.01 and ION2019 calculations for the standard RPC AD1 cloud model considered in this work.

central AD for $C_f=0.3$. According to BLS14, the observed Ly α and C IV 1549 luminosities are consistent with this covering factor but this is not the case for H β whose calculated equivalent width (EW) is a factor 3-4 below the mean observed value. This issue is not discussed further in their work except for commenting on the difficulty in calculating reliable Balmer line intensities.

The difficulty in reproducing the observed luminosity of H β and other Balmer lines has been addressed by Kaspi & Netzer (1999) in their MPC modeling of the spectrum of NGC 5548. This was attributed to inadequate treatment of such lines in photoionization models where radiative transfer is based on the local escape probability method. Lawther et al. (2018) repeated most of the Kaspi & Netzer (1999) calculations and applied them to the 2014 data of NGC 5548. They also added a detailed discussion of the bound-free diffuse continuum (hereafter DC) which was not included in Kaspi & Netzer (1999), and noted that the calculated $L(\text{H}\beta)$ is much weaker than observed. As shown below, the new RPC and MPC calculations show a similar discrepancy with H β and H α observations.

3.3 New RPC and MPC calculations

The aim of the present work is to use observed line luminosities, and line lags, in order to test and constrain RPC and MPC cloud models. The emphasis is on *pure* models, i.e. those where either $P_{\text{rad}} \gg P_{\text{mag}}$ or $P_{\text{mag}} \gg P_{\text{rad}}$. More realistic BLRs would probably contain clouds of both types, for example RPC clouds in the inner BLR and MPC clouds in the outer BLR.

As explained, RPC cloud models require 5 parameters for a given L_{AGN} , SED and gas composition. All the radial parameters can be expressed relative to $R_{\text{H}\beta}$, defined

as the RM distance of the $H\beta$ line: $R_{H\beta}=34[L_{5100,44}]^{1/2}$ ld. The total line luminosities are obtained by integrating from $R_{in}=0.2R_{H\beta}$ to $R_{out}=4R_{H\beta}$ and the line emission is assumed to be strongly suppressed, by the torus dust, at larger distances. For each case I used eqn. 1 with a large range of the covering factor parameter p , between 1 and 3.5, normalized to give a total covering factor of 0.4. This was considered to be the largest covering factor which is still consistent with the assumption of no shadowing of one cloud by another.

For each model and each line, I calculated the mean emissivity radius which is assumed to represent the measured RM distance of the line. As explained in various earlier works (e.g. Bottorff et al. 2002), the mean emissivity radius can differ from the responsivity distance which is more closely related to the peak of the cross correlation function (CCF) between the line and continuum light curves. The mean emissivity radius depends on line responsivity and also on the duration of the driving continuum pulse (e.g. Goad & Korista 2015). Here I assume that the mean measured RM distances in the RM-sample are based on long duration driving continuum events and are therefore similar to the mean emissivity weighted radii.

There are several differences between the new MPC calculations presented here and the earlier ones applied to NGC 5548. The first is the constant pressure assumption (some earlier calculations assumed constant gas density). The second is the lower limit on the gas density at the illuminated face of the clouds imposed by the radiation pressure force. To take this into account, I assumed $P_{mag} \propto R^{-s}$, and adjusted the density at the illuminated face such that $P_{mag} > P_{rad}$ at R_{in} . I also assumed $s < 2$ thus $P_{mag} > P_{rad}$ throughout the BLR. This normalization is not the only possibility and there can be cases where P_{rad} dominates over the inner BLR and P_{mag} further out. Such cases were not considered. An additional difference from the earlier calculations is the neglect of the requirement that individual clouds retain their mass as they move in or out. This requirement sets the column density as a function of distance and also allowed some clouds to become optically thin close to the central source (for details see Netzer 1990). All clouds in the present paper have the same large column density of $10^{23.5} \text{ cm}^{-2}$. The covering factor dependence is set solely by the parameter p in eqn. 1

All MPC cloud models presented below assumes $s = 1$. The relatively small change in gas temperature at the illuminated face over a large range of distances shows that, to a good approximation, $n_H \propto R^{-0.95}$ and $U \propto R^{-1.05}$.

4 COMPARISON WITH OBSERVATIONS

The results presented here pertain to two cases: RM-sample AGN and the specific case of NGC 5548.

Table 2. Mean observed broad emission line luminosities and distances for RM-sample AGN with monochromatic luminosity of $L_{5100}=10^{43} - 10^{45} \text{ erg s}^{-1}$.

Line	Luminosity (erg s^{-1})	Relative intensity	distance (ld)	Relative distance
$H\beta$	$0.018 L_{5100}$	1	$34[L_{5100,44}]^{1/2}$	1
$Ly\alpha$		5-20		0.4-0.8
$H\alpha$		2-4		1-1.3
$P\alpha$		0.3-0.4		1(?)
$C\text{IV}1549$		4-15		0.4-0.8
$\text{He II } 1640$		0.5-2		0.2-0.5
$\text{Mg II } 2798$		0.5-3		1-1.5
$C\text{III}]_{\text{Sim}} 1900$		2-4		?
$\text{O VI } 1035$		1-3		?
Graphite dust		100-400		3 - 4

4.1 RM-sample AGN

This set of calculations is aimed to compare RM results, and broad emission line luminosities, with the mean properties of the RM-sample AGN presented in Kaspi et al. (2000) and Bentz et al. (2013). The mean observed line luminosities and lags are collected from the literature and are listed in Table 2. The main references are: Netzer (1990), Netzer et al. (1995), Kaspi et al. (2000), Telfer et al. (2002), Kim, Im & Kim (2010), Bentz et al. (2010), Bentz et al. (2013), Lira et al. (2018), Pei et al. (2017) and Kriss et al. (2019). The line luminosities are normalized to $L(H\beta)$, and the line lags to $R_{H\beta}/c$. They show a large scatter which is mostly intrinsic and related to different phases of activity, different SED shapes, different continuum variability time scales, disk inclinations and accretion rates. The table lists also the mean luminosity of the $P\alpha$ line and the following calculations add the predicted $\text{Br}\gamma$ line. This is necessary in order to compare with coming GRAVITY observations that can measure both of these lines in the K-band. The listed time-lag for the line is not measured by RM experiments but rather deduced from the similarity of the $H\beta$ and $P\alpha$ line profiles.

In general, the line intensity ratios do not depend strongly on L_{AGN} (no line reddening is assumed); an important issue which was discussed in numerous earlier publications (e.g. Netzer & Davidson 1979; Netzer et al. 1995; Baron et al. 2016, and references therein) and addressed in §5 below.

The new calculations pertain to two different scenarios: fixed boundaries BLRs and changing boundaries BLRs.

4.1.1 Fixed boundaries BLRs

This set of calculations assumes that R_{in} and R_{out} do not change as the source luminosity increases or decreases. For the RPC clouds I follow the approach of BLS14 and start the integration into the cloud assuming a density well below the critical density corresponding to $P_{rad}=P_{gas}$. This translates to $U = 1 - 10$. The calculations stop at $N_{col}=10^{23.5} \text{ cm}^{-2}$ but this number is somewhat arbitrary since the ionized column in all cases does not exceed $10^{23.3} \text{ cm}^{-2}$. The covering factor of individual clouds are very small (the *open geometry* option in *cloudy*) and no obscuration of one cloud by

another is considered. The covering factor parameter, p , is allowed to vary in the range 1-3.5. The larger this parameter is the smaller is the emissivity weighted radius. In general, p is the most important parameter in determining the mean emissivity radii of the lines.

Fig. 3 shows results for the three main models: RPC-AD1, RPC-AD2 and MPC-AD1. In all cases $C_f=0.4$. The calculations are compared with the luminosities and lags shown in Table 2 (marked as magenta crosses in all panels). Table 3 provides more information for those values of p which results in the closest agreement with $R_{H\beta}$: 2.4 for the RPC-AD1 model and 2.3 for the MPC-AD1 model. It also shows calculations for $p = 1.2$ that results in longer lags for all lines and and for a RPC model with metallicity which is three times solar. Given the observational uncertainties, and intrinsic scatter, all the results in the range $p = 2.2 \pm 0.5$ are consistent with all mean lags. The time lags for the Balmer and Paschen continua and O VI 1035 are not known. However, their luminosities per unit covering factor are almost constant with distance, similar to the case of He II 1640 (Fig. 2). This means that the line efficiency factor, $\epsilon(R)$, depends very weakly on R . Because of this, the calculated lags are also similar to those of the He II lines.

I have also calculated RPC models for the powerlaw SED shown in Fig. 1. The results are very similar to those of the AD1 SED in all respects. The preferred covering factor parameter in this case is somewhat smaller, $p = 2.2$, which reflects the fact that the ionizing luminosity of this SED, which dominates the radial distribution of the clouds, is somewhat smaller than in AD1 (see Table 1). The results of this case are not discussed further in this work.

Unlike the time lags, there is a serious disagreement, which is clearly visible in Fig. 3 and Table 3, between the observed and calculated $H\beta$ luminosity, regardless of the value of p . A similar discrepancy is found for $H\alpha$, $P\alpha$ and $H\gamma$ (not shown in the diagram). BLS14 studied the case of $C_f=0.3$ and did not calculate mean emissivity radii. They also noted the $H\beta$ deficiency. A similar problem was found in the earlier NGC 5548-MPC calculations of Kaspi & Netzer (1999) and also in Lawther et al. (2018). Below I refer to this discrepancy as the ‘‘Balmer lines crisis’’.

The covering factor used in this work is the largest which is still consistent with the assumption of no cloud obscuration. The models assume isotropic ionizing continuum yet some BLRs are likely to form a rotating system around the mid-plane of the AD where the ionizing photon flux can be very different (see e.g. the new GRAVITY observations of 3C 273 by Gravity Collaboration et al. (2018)). This could increase the discrepancy between the observed and the calculated Balmer line luminosities. The exact magnitude of this effect depends on BH mass and spin (see Laor & Netzer 1989, figures 7 & 8). An additional factor which is not addressed here is the uneven emission from the illuminated and dark sides of the clouds.

A major finding of this work is that, contrary to the Balmer lines crisis, there is no luminosity crisis for Ly α , CIV 1549, the two He II lines (note that

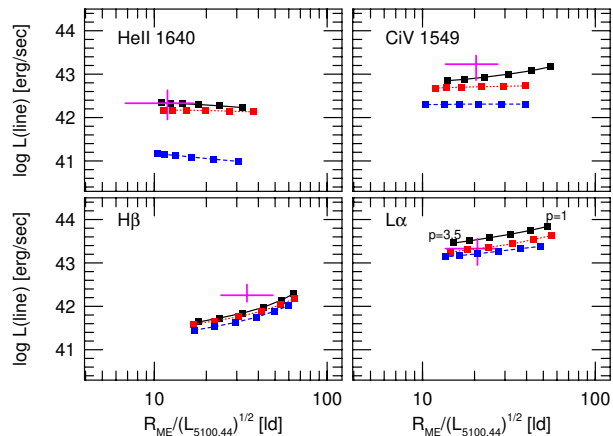


Figure 3. Luminosities and mean emissivity radii for four BLR lines, $C_f=0.4$ and a range of covering factor parameter p (marked along the lines and decreasing from $p = 3.5$ (left) to $p = 1$ (right)). *Solid lines*: RPC model, AD1 SED. *Dashed lines*: RPC model, AD2 SED. *Dotted lines*: MPC model, AD1 SED. The estimated observational uncertainties are given by the central cross in each panel. Note that none of the models can reproduce the mean observed $L(H\beta)$ despite the large covering factor. The weak ionizing continuum AD2 SED fails also to explain $L(He II 1640)$ and $L(C IV 1549)$.

He II 1640/He II 4686 ≈ 10) and O VI 1035. In fact, the calculated luminosities are consistent with a large range of covering factor from 0.1 to 0.4. The calculated luminosities of the Mg II 2798 blend, and the 1900Å blend (a combination of C III] 1909 and Si III] 1893), in solar composition gas, are considerably smaller than the ones observed. Much of this discrepancy is cured when higher metallicity is used. Unfortunately, there are no reliable measurements of the lags of these lines.

4.1.2 Changing boundaries BLRs

A large increase in L_{AGN} can result in dust sublimation and a different outer boundary provided the sublimation time can be neglected (Baskin & Laor 2018). Such an event results in additional line emission and a change in the mean emissivity radius. The effect on R_{in} is more difficult to assess, in particular in those cases where the time scale of the variations is shorter than the dynamical time at R_{in} . One possibility is that radiation bounded clouds close to R_{in} will become partly transparent thus reducing the efficiency of the lines from the more neutral species.

In this section I investigate RPC and MPC cloud models where L_{AGN} increases by a factor 2, R_{out} increases by $2^{1/2}$, and there is no change in R_{in} . Since the two types of models lead to similar results, I focus on RPC models. Fig. 4 shows dL/dR for several lines, and the Balmer continuum, in the $p = 2.4$ RPC case, before (solid lines) and after (dashed

lines) such an increase. The lines emission after the change start at the same R_{in} and extend all the way to the new R_{out} . The integrated old and new luminosities and lags are listed in Table 4.

Table 3. Calculated luminosities and lags relative to $L(\text{H}\beta)=0.018L_{5100} \text{ erg s}^{-1}$ and $R_{\text{H}\beta}=34[L_{5100,44}]^{1/2} \text{ ld}$, for RPC and MPC models with AD1 SED. Numbers in parentheses are for 3×solar metallicity gas.

Line	RPC $p = 2.4$		RPC $p = 1.2$		MPC $p = 2.3$		MPC $p = 1.2$	
	Relative luminosity	Relative distance	Relative luminosity	Relative distance	Relative luminosity	Relative distance	Relative luminosity	Relative distance
H β	0.38 (0.36)	1 (1)	0.91	1.79	0.36	1	0.75	1.77
Ly α	20.8 (19.7)	0.75 (0.76)	34.6	1.43	13.6	0.80	21.9	1.48
H α	0.97 (0.88)	1.16 (1.16)	2.72	1.93	0.78	1.12	1.81	1.86
P α	0.06 (0.056)	1.16 (1.14)	0.17	1.97	0.07	1.14	0.17	1.90
Br γ	0.009 (0.009)	0.82 (0.82)	0.016	1.73	0.015	0.83	0.025	1.59
C iv1549	5.5 (4.63)	0.70 (0.61)	8.5	1.43	2.82	0.54	2.95	1.02
He II 1640	1.2 (0.93)	0.44 (0.45)	1.0	0.87	0.81	0.49	0.77	0.96
Mg II 2798	0.21 (0.35)	1.06 (0.99)	0.52	1.9	0.52	1.20	1.32	1.97
C III] + Si III] 1900	0.45 (0.99)	1.49 (1.24)	1.64	2.1	0.18	1.18	0.45	1.95
O VI 1035	2.61 (2.06)	0.49 (0.48)	2.58	1.0	0.06	0.29	0.03	0.38
Balmer cont.	32.0 (30.9)	0.48 (0.48)	30.6	0.92	39.8	0.53	40.4	0.99
Paschen cont.	22.4 (20.2)	0.45 (0.45)	20.1	0.87	24.6	0.48	22.4	0.88

Table 4. Luminosities and lags due to a luminosity increase by a factor 2. In both cases the SED is AD1 and $p = 2.4$. Line luminosities and lags are relative to the nominal values for H β listed in Table 3.

Line	$L_{5100}=10^{44} \text{ erg s}^{-1}$		$L_{5100}=2 \times 10^{44} \text{ erg s}^{-1}$	
	Luminosity	Lag	Luminosity	Lag
H β	0.38	1	0.55	1.24
Ly α	20.8	0.75	30.9	0.93
C iv1549	5.5	0.70	8.9	0.81
He II 1640	1.2	0.44	2.35	0.47
Balmer cont.	32.0	0.48	62	0.51

Table 5. Observed and calculated luminosities and lags for the RPC model of NGC 5548. Luminosities are relative to $L(\text{H}\beta)=4.5 \times 10^{41} \text{ erg s}^{-1}$ and lags relative to 16 ld. The assumed dust sublimation radii are: $R_{\text{out}}(1)=49 \text{ ld}$ and $R_{\text{out}}(2)=86 \text{ ld}$.

Line	$R_{\text{out}}(1) \ p = 1.8$			$R_{\text{out}}(2) \ p = 1.8$	
	Observed luminosity	Calculated luminosity	Calculated lag	Calculated luminosity	Calculated lag
H β	1	0.18	1	0.21	1.4
Ly α	8.96	5.5	0.77	5.7	0.98
H α	3.7	0.55	1.27	0.72	1.96
C iv1549	8.96	4.2	0.67	4.3	0.84
He II 1640	1.10	1.1	0.44	1.1	0.52
Mg II 2798	1.5	0.21	1.07	0.25	1.59
Balmer cont.		11.5	0.31	11.3	0.36
Paschen cont.		8.7	0.37	8.6	0.42

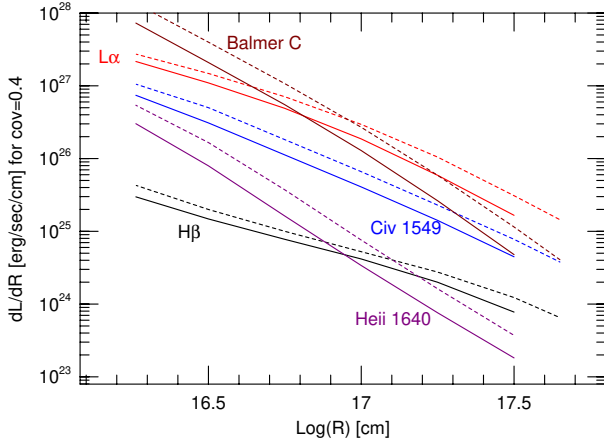


Figure 4. Line and bound-free continuum luminosities in response to an AD1 SED with $p = 2.4$: $L_{5100}=10^{44}$ erg s $^{-1}$ (solid lines) and $L_{5100}=2 \times 10^{44}$ erg s $^{-1}$ (dashed lines).

There are two important things to note. The local (same R) response of different lines is very different representing the different emission coefficient $\epsilon(R)$ (§2). Most noticeable is the large difference between the small increase in $L(H\beta)$ compared with the much larger changes in $L(He II 1640)$ and $L(\text{Balmer continuum})$. Unfortunately, it is not at all clear whether the change in $L(H\beta)$ can be trusted given the problem in calculating, reliably, the intensity of this line.

A second and related aspect is the very different change in R_{ME} for the different lines. The largest relative changes are in those lines whose luminosity per unit covering factor increase outwards ($H\beta$ and $Ly\alpha$, see also Fig. 2). Even for these lines, the increase in R_{ME} is smaller than the naively expected change by a factor $2^{1/2}$. This is related to the specific value of $p = 2.4$ which emphasizes the inner parts of the BLR, and to the fact that R_{in} was not allowed to change (eqn. 2). Thus $L(He II 1640)$ and $L(\text{Balmer continuum})$ increase by a factor of ~ 2 at all distances but their mean emissivity radii hardly change.

Models with smaller p , e.g. the case of $p = 1.2$ shown in Table 3, give more weights to the outer parts of the BLR. In such cases, the changes in R_{ME} are larger and approach $2^{1/2}$. However, such models fail to reproduce the mean emissivity radii of $Ly\alpha$, C IV 1549, He II 1640 and the Balmer lines. All these predictions could be tested against observations.

4.2 The BLR in NGC 5548

The most detailed studies, so far, involve the intermediate luminosity AGN NGC 5548. This object was the target of three very large optical-UV campaigns, in 1989, 1993 and 2014, and a large number of additional spaceborne and ground-based campaigns (see Pei et al. 2017; Korista & Goad 2019; Kriss et al. 2019, and references

therein). Except for several years of very low luminosity, which will not be discussed here, the SED is dominated by a strong X-ray continuum which is substantially different from the three other SEDs studied in this work. Details and a plot of this SED are provided in §3.1.

The large number of RM campaigns provide an opportunity to compare the RPC cloud model for this source with published LOC and MPC models. Extensive discussions of the BLR response in this source, in the framework of the LOC model, are given in Goad & Korista (2015) and Korista & Goad (2019). These studies addressed density, column density and luminosity dependencies as well as the effect of the dusty torus location on the observed line luminosities and lags. They also addressed the luminosity and lag of the bound-free continuum. For various MPC models see Kaspi & Netzer (1999) and Lawther et al. (2018).

The RPC clouds model presented here were applied to the luminosity and SED of NGC 5548 during 2014. I used the line and continuum observations described in Lawther et al. (2018), Pei et al. (2017) and Kriss et al. (2019) and assumed the SED properties detailed in §3.1. Using the Bentz et al. (2013) normalization, $R_{H\beta} \approx 16$ ld, about twice the lag measured during the STORM 2014 campaign and close to the 25-year mean for this source (Pei et al. 2017). According to Korista & Goad (2019), the much shorter lags (a factor of ~ 2) observed in 2014 are consistent with the very different continuum variability time scale during this campaign (see Fig. 7 in their paper).

Using the above SED, I calculated emissivity-weighted radii and luminosities for the strong BLR lines, and the bound-free continua, under two assumptions about the dust sublimation radius: $R_{out}=49$ ld and $R_{out}=86$ ld. These bracket the estimated R_{out} based on dust RM. These values are 2-3 times smaller than the radius considered by Goad & Korista (2015) and Korista & Goad (2019) who investigated different BLR and torus geometries, and the changes of the sublimation radius in response to continuum variations. The LOC models used in these papers assumed $p = 1.2$. The main reason for the very large R_{out} , and the small p , is the too small $L(H\beta)$ predicted by the model compared with the observations. These assumptions resulted in stronger Balmer lines and smaller $L(Ly\alpha)/L(H\beta)$. As before, $C_f=0.4$.

The results of the new calculations are presented in Table 5 alongside the mean observed line luminosities taken from the 1989 and 2014 optical-UV campaigns. I chose $p = 1.8$ which gives $R_{H\beta}=16$ ld for $R_{out}=49$; the mean observed lag for this L_{5100} . For $R_{out}=86$ ld and $p = 1.8$ I find $R_{H\beta}=22$ ld. The calculated luminosities and lags are in good agreement with the observations for $Ly\alpha$, C IV 1549 and He II 1640. However, this is not the case for the Balmer lines and the Mg II 2798 blend. The lags for these lines are in good agreement with the observations but the luminosities are about a factor 4-5 too small. This is in line with the Balmer lines crisis mentioned earlier.

I have also experimented with super-solar metallicity, increasing the metal abundance by a factor 3. This increased

the Mg II 2798 luminosity by about a factor 2 but made little difference for the other lines and continua.

5 DISCUSSION

5.1 A comparison of RPC and MPC models

The new calculations presented here pertain to simplified scenarios where *all clouds* in the BLR are controlled either by radiation pressure or by external magnetic pressure. Real BLRs probably include some mixture of the two, depending on distance from the BH, position relative to the central disk, etc. I also neglected the possibility that some clouds, especially at small distances, are not ionization bounded. Nevertheless, identifying the main features of the two *pure* cases is important for the understanding of the BLR physics.

Perhaps the most important feature of the RPC clouds model is the fact that compression by radiation pressure force is unavoidable when $P_{rad} \geq P_{gas}$. This sets the run of temperature and density across the cloud and hence the emergent line and continuum flux. It also results in a smaller number of parameters compared with the LOC and MPC cloud models. Given radiation pressure force, most earlier LOC and MPC models must be modified in a significant way. In particular, in typical AGN SEDs, the radiation pressure force restricts the range of allowed densities in pure LOC and MPC models. For example, in the RM-sample model with the AD1 SED, the lowest allowed density for which $P_{gas} > P_{rad}$ is about $10^{11} [(7\,ld)/R]^2\,\text{cm}^{-3}$. Gas with lower density will be compressed on a short time scale and, perhaps, blown out of the system.

Large column density RPC clouds are characterized by an almost constant U at the hydrogen ionization front, regardless of R . This behaviour can explain the great spectral similarity between AGN of very different luminosities, and the different lags of some of the lines like the Balmer lines, Ly α , C IV 1549 and the He II lines. An additional feature is the large range of ionization parameters inside the clouds. This allows to obtain strong lines of highly ionized and less ionized species from the same location. For example, it helps to explain the good agreement between the predicted and observed luminosity of the O VI 1035 line. Unfortunately, the mean emissivity radius of this line has never been observed by RM experiments and hence cannot be used to test this prediction.

The situation regarding the luminosity of low ionization lines like Mg II 2798 and the optical Fe II lines, and their (rather uncertain) lags, is not as clear. The observed line luminosities seem to indicate a drop of U with distance from the central source, which is less consistent with the RPC model. This is not entirely clear because of the dependence on gas metallicity. It may also indicate that realistic BLR models must include a mixture of RPC and MPC clouds.

RPC cloud models require a narrow range of covering factor parameters, $p \approx 2.2 \pm 0.5$. Smaller values that were used in the past seem to be in contradiction with line and dust RM measurements and with K-band interferometry.

This range of p can explain the measured lags of *all* broad lines with reliable RM measurements.

Magnetic pressure confined clouds have been investigated in several earlier works (Rees et al.; 1989, Goad et al. 1993; Kaspi & Netzer 1999, Lawther et al. 2018). Here the number of free parameters is 5 or 6, depending on whether or not the clouds retain their identity as they move around the BH. The present calculations are different from the earlier ones in two ways. First, p is larger than in earlier works. Second, I only consider MPC clouds for which $P_{mag} \gg P_{rad}$ at the illuminated face. For the case demonstrated here, with $P_{mag} \propto R^{-1}$, the line luminosities and lags are similar to those of the RPC clouds model for some of the lines (He II 1640, Ly α , C IV 1549) and different for others (Mg II 2798). The largest difference is for the O VI 1035 line blend which is under-luminous in the present MPC models because of the lower ionization parameter. A similar effect was noted by Stern et al. (2016) who calculated the luminosity of the Ne VIII 774 blend in cases where P_{rad} is the dominated external pressure and compared them with cases where external, hot gas pressure is more important. Obviously, there is a range of possible radial dependencies of P_{mag} that are different from the one considered here. There is also an uncertainty associated with the exact P_{rad}/P_{mag} at different locations inside the BLR.

In conclusion, the main advantage of RPC cloud models is the smaller number of model parameters and the fact that radiation pressure must operate at all locations, even if not as the dominant source of pressure. Both RPC and MPC models can reproduce the observed lags for all broad emission lines with reliable RM measurements and neither can explain the observed luminosities of the Balmer lines.

5.2 What is the origin of the Balmer lines crisis?

For $p = 2.2 \pm 0.5$, both the calculated luminosities and lags of Ly α , H II 1640 and C IV 1549 are consistent with the observations. The agreement is not as good for the L(Mg II 2798) but most of the discrepancy can be cured by resorting to higher metallicity gas. In contrast, the calculated H α , H β and P α luminosities are too weak by factors of 2-5 despite the very good agreement between the observed and the calculated mean emissivity radii. A similar discrepancy was found by Kaspi & Netzer (1999) in their study of NGC 5548, and later confirmed by Lawther et al. (2018). The new calculations verify and extend this finding to more physically consistent models.

BLR clouds are very optically thick in many Balmer and Paschen lines. In the models considered here, $\tau(\text{H}\beta) = \text{few} \times 10^3$. Unlike resonance lines, like Ly α , where most of the scattering of the line photons is taking place close to their place of origin, the non-resonance Balmer line photons can propagate through the cloud before escaping the gas. This can affect the $n > 1$ level populations, and the local gas temperature, in a way that is difficult to simulate properly by models like *cloudy* and ION which use the local escape probability formalism.

It is worth noting in passing that the relative intensities of $H\alpha$, $H\beta$ and $P\alpha$ are similar to what is predicted from LTE calculations with a Boltzmann level populations. This was noted in earlier works which discussed the observed Balmer line ratios in AGN in the context of the Boltzmann plot often used to analyze optically thin plasma (Popović 2003; Ilić et al. 2012). The inclusion of $Ly\alpha$ clearly shows a large discrepancy between such calculation and the observed hydrogen line spectrum; the direct result of the very large optical depth of the lines.

A related issue is the luminosities of the various bound-free continua. In the models calculated here, the optical depth at the Balmer limit is less than 10 and the one at the Paschen limit less than 1. Thus transfer is not likely to be important. Some confirmation of this is the measured $L(\text{Balmer cont.})/L(Ly\alpha)$ which was found by Wills, Netzer & Wills (1985) to be of order unity, similar to the RPC and MPC model predictions listed in Table 3.

In conclusion, it seems that the escape of Balmer and Paschen line photons from high density, large optical depth BLR clouds, is more efficient than calculated by *cloudy* and by ION. Other lines and continua are less affected.

The discrepancy discussed here is related to the long-standing problem of the relative intensity of the Lyman and Balmer lines in AGN spectra (see e.g. Netzer & Davidson 1979; Netzer et al. 1995, and references therein). The conclusions reached here are based on more physically motivated photoionization models and supported by additional observational constraints provided by numerous RM studies not available for the earlier studies.

Alternative explanations for the too strong (compared with calculations) $H\beta$ line, or equivalently too small $Ly\alpha/H\beta$, involve line and/or continuum reddening (e.g. Netzer et al. 1995; Baron et al. 2016). This cannot solve the entire problem because reddening involves more luminous intrinsic ionizing continuum which results in larger R_{ME} for many lines.

It is hard to estimate what will be the effect of including a more realistic transfer method on the intensities of other emission lines. In particular, how will the energy redistribute inside the cloud. The lines that are most likely to deviate from what was found here are $Mg II$ and $Fe II$ lines that are produced in the low ionization parts of the clouds. Lines that originate from the more highly ionized parts are in much better agreement with the observations and, perhaps, less likely to be affected.

Finally, a comment on the mean emissivity radius of the *total* emission from the BLR. This can be estimated, quite accurately, by noting that all the ionizing radiation is absorbed by the large column density clouds considered here, as well as some of the incident radiation between 0.25 and 1 Ryd. This is almost independent of the cloud locations. The calculations show that for $p = 2.4$, $R_{ME}(\text{total BLR emission}) \approx 0.5 R_{ME}(H\beta)$. This is a factor 6-8 smaller than R_{out} . Thus, a prediction of the RPC cloud model is that most of the flux emitted by the clouds is at very small distances compared with the dust sublimation radius. A large

fraction of this radiation is due to various bound-free continua, which are discussed in the next section.

5.3 Diffuse continuum emission from the BLR

Recent studies clearly indicate that long wavelength continuum variations lag the variable UV continuum in a wavelength dependent way. This was interpreted in several publications as a delayed response of a centrally illuminated accretion disk to luminosity variations of the central source. Modeling suggests that the derived AD size is some 2-4 times larger than the size of standard ADs such as the ones assumed here (e.g. Edelson et al. 2019, and references therein). Such ideas have been challenged by new observations, and new calculations, of the diffuse continuum (DC) from the BLR. Several recent BLR calculations show that such emission can cause much, perhaps all of the observed effect (Lawther et al. 2018; Chelouche, Pozo Nuñez & Kaspi 2019; Korista & Goad 2019). Thus the origin of the DC is crucial for the understanding of both the BLR physics and the properties of the central disk.

An important new result is that $R_{ME}(\text{Balmer continuum})$ and $R_{ME}(\text{Paschen continuum})$ in the RPC and MPC cloud models are significantly smaller than $R_{H\beta}$. For $p = 2 - 2.5$ they correspond to $\sim 0.5 R_{H\beta}$. For the covering factor considered here (0.4) and the AD1 and AD2 continua, the DC contribution to the total emitted 2500-10000Å flux is very significant, ranging between 30 and 90%. This is similar to what has been proposed by Chelouche et al. 2019 for the case of MK 279. The relative DC contributions for the power-law and NGC 5548 SEDs are smaller because in these cases the optical continuum is stronger relative to ionizing continuum which determines the DC luminosity. This explains much of the difference between the relative DC contributions calculated here and the ones shown in Lawther et al. (2018) and Korista & Goad (2019).

Fig. 5 shows the DC continuum for the generic RM-sample AGN. In this case I assumed that a single RPC cloud at a distance of 17 ld ($R_{ME}(\text{Balmer continuum})$ in Table 3) from an AD with $L_{5100} = 10^{44} \text{ erg s}^{-1}$, is an adequate representation of the entire DC emission. The diagram shows the incident AD1 continuum and two possibilities for the DC spectrum, one representing a spherical cloud distribution (middle solid line) and one a thick disk-like BLR seen from the side (upper dashed line). The differences are due to the fact that in the spherical situation, both the incident continuum and the diffuse emission are attenuated on their way to the observer. As seen from the diagram, the DC adds about 40% to the AD continuum at 3000Å, about 60% at 5000Å and about 90% at 7700Å. Naively, such a DC flux would result in a combined AD+DC continuum time lag at 5000Å of about $6[L_{5100,44}]^{1/2}$ days if the AD variations are wavelength independent (see more explanation in Chelouche et al. 2019). The combined continuum time lags are significant even at smaller covering factors. Given these assumptions, the lags are similar to the optical continuum lags

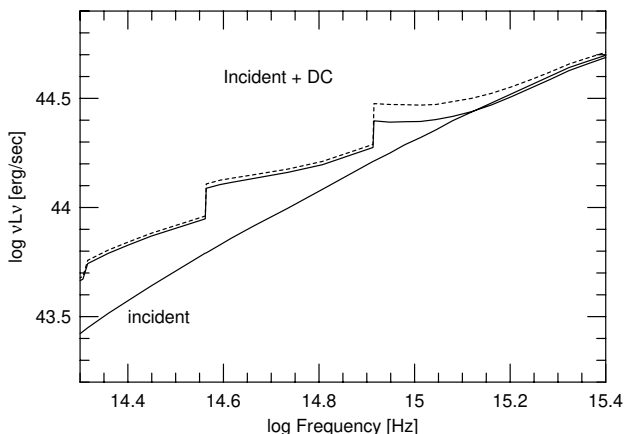


Figure 5. Diffuse continuum emission from a RPC-dominated BLR. In this case the SED is AD1, $L_{5100}=10^{44}$ erg s $^{-1}$, the cloud is at R_{ME} (Balmer continuum) and the covering factor is 0.4. The bottom solid line is the incident AD continuum, the middle solid line is the observed emission from a spherical cloud distribution, and the upper dashed line is a side view of the total emission for a flat rotating BLR (broad emission lines are not plotted for clarity).

reported in Edelson et al. (2019), (Fausnaugh et al. 2017), and other cases.

While the role of DC emission from the BLR must be studied more carefully in individual sources, and calibrated against observed line and continuum intensities and SED shapes, it is important to emphasize that such DC contributions, and lags, are unavoidable. Moreover, in low luminosity AGN, neglecting to account for this emission will lead to an unrealistically strong stellar contribution to the total observed continuum.

6 CONCLUSIONS

This paper presents new photoionization models in attempt to reproduce the observed luminosities and lags of the strongest broad emission lines in AGN. There are 4 different SEDs and two types of models: radiation pressure confined (RPC) clouds and magnetic pressure confined (MPC) clouds. The main results are:

(i) The observed lags of Ly α , H β , H α , C IV 1549, and He II 1640 are reproduced by both RPC and MPC cloud models provided the covering factor parameter p ($dC_f \propto R^{-p}dR$) is in the range 2-2.5. This is also the case for the Mg II 2798 and Fe II lines whose lags are more uncertain.

(ii) The observed luminosities of Ly α , C IV 1549, He II 1640, and O VI 1035, are well reproduced by RPC clouds models with ADs and powerlaws SEDs. The MPC clouds model is not as successful in reproducing the

luminosities of the higher ionization lines. The luminosities of Mg II 2798 and the 1900Å blend of C III] and Si III] lines approach their observed values for super solar metallicity gas.

(iii) The calculated Balmer and Paschen line luminosities fall short of the observed luminosities by factors of 2-5. This is interpreted as a failure of the escape probability formalism used in *cloudy* and ION to properly calculate those lines in high density, large optical depth gas.

(iv) The predicted (and often observed) short-time changes of the mean emissivity radii of strong emission lines in proportion to $L_{AGN}^{1/2}$ require corresponding changes in both R_{in} and R_{out} .

(v) The Balmer and Paschen bound-free continua are very strong in all models. Their mean emissivity radii are about half the mean emissivity radius of the Balmer lines. These continua add substantially to the continuum emission of the central source at all wavelengths between 2500 and 10000Å. This must be taken into account when interpreting the results of continuum RM experiments.

7 ACKNOWLEDGMENTS

I am grateful to Ari Laor, Alex Baskin, Jonathan Stern, Kirk Korista and Mike Goad for useful comments. I also thank the referee for helping to clarify several important issues in this work.

REFERENCES

- Baldwin J., Ferland G., Korista K., Verner D., 1995, The Astrophysical Journal, 455
- Baron D., Stern J., Poznanski D., Netzer H., 2016, ApJ, 832, 8
- Baskin A., Laor A., 2018, MNRAS, 474, 1970
- Baskin A., Laor A., Stern J., 2014, MNRAS, 438, 604
- Bentz M. C. et al., 2013, ApJ, 767, 149
- Bentz M. C. et al., 2010, ApJ, 716, 993
- Bottorff M. C., Baldwin J. A., Ferland G. J., Ferguson J. W., Korista K. T., 2002, The Astrophysical Journal, 581, 932
- Chelouche D., Pozo Nuñez F., Kaspi S., 2019, Nature Astronomy, 3, 251
- Dexter, J. et al., 2020, arxiv arXiv:1910.00593
- Dopita M. A., Groves B. A., Sutherland R. S., Binette L., Cecil G., 2002, The Astrophysical Journal, 572, 753
- Du P. et al., 2015, ApJ, 806, 22
- Edelson R. et al., 2019, ApJ, 870, 123
- Fausnaugh M. M. et al., 2017, ApJ, 840, 97
- Ferland G. J. et al., 2017, Revista Mexicana de Astronomía y Astrofísica, 53, 385
- Goad M. R., Korista K. T., 2015, MNRAS, 453, 3662
- Goad M. R., O'Brien P. T., Gondhalekar P. M., 1993, Monthly Notices of the Royal Astronomical Society, 263, 149
- Gravity Collaboration et al., 2018, Nature, 563, 657

- Grier C. J. et al., 2017, *ApJ*, 851, 21
- Hu C. et al., 2015, *ApJ*, 804, 138
- Ilić D., Popović L. Č., La Mura G., Ciroi S., Rafanelli P., 2012, *A&A*, 543, A142
- Kaspi S., Netzer H., 1999, *The Astrophysical Journal*, 524, 71
- Kaspi S., Smith P. S., Netzer H., Maoz D., Jannuzi B. T., Givon U., 2000, *ApJ*, 533, 631
- Kim D., Im M., Kim M., 2010, *The Astrophysical Journal*, 724, 386
- Korista K., Baldwin J., Ferland G., Verner D., 1997, *The Astrophysical Journal Supplement Series*, 108, 401
- Korista K. T., Goad M. R., 2000, *ApJ*, 536, 284
- Korista K. T., Goad M. R., 2019, *MNRAS*, 489, 5284
- Koshida S. et al., 2014, *ApJ*, 788, 159
- Kriss G. A. et al., 2019, *The Astrophysical Journal*, 881, 153
- Laor A., Netzer H., 1989, *MNRAS*, 238, 897
- Lawther D., Goad M. R., Korista K. T., Ulrich O., Vestergaard M., 2018, *MNRAS*, 481, 533
- Lira P. et al., 2018, *ApJ*, 865, 56
- Mehdipour M. et al., 2015, *A&A*, 575, A22
- Mor R., Netzer H., 2012, *MNRAS*, 420, 526
- Netzer H., 1990, 20. Saas-Fee Advanced Course of the Swiss Society for Astrophysics and Astronomy: Active galactic nuclei
- Netzer H., 2013, *The Physics and Evolution of Active Galactic Nuclei*
- Netzer H., 2015, *AnnRevAstAp*, 53, 365
- Netzer H., Brotherton M. S., Wills B. J., Han M., Wills D., Baldwin J. A., Ferland G. J., Browne I. W. A., 1995, *ApJ*, 448, 27
- Netzer H., Davidson K., 1979, *MNRAS*, 187, 871
- Netzer H., Laor A., 1993, *ApJL*, 404, L51
- Netzer H., Marziani P., 2010, *ApJ*, 724, 318
- Pei L. et al., 2017, *ApJ*, 837, 131
- Popović L. Č., 2003, *ApJ*, 599, 140
- Rees M. J., Netzer H., Ferland G. J., 1989, *The Astrophysical Journal*, 347, 640
- Slone O., Netzer H., 2012, *MNRAS*, 426, 656
- Stalevski M., Fritz J., Baes M., Nakos T., Popović L. Č., 2012, *MNRAS*, 420, 2756
- Stern J., Faucher-Giguère C.-A., Zakamska N. L., Hennawi J. F., 2016, *ApJ*, 819, 130
- Telfer R. C., Zheng W., Kriss G. A., Davidsen A. F., 2002, *ApJ*, 565, 773
- Wills B. J., Netzer H., Wills D., 1985, *ApJ*, 288, 94